Nigerian Research Journal of Engineering and Environmental Sciences 7(1) 2022 pp. 54-68
p ISSN: 2635-3342; e ISSN: 2635-3350

Nigerian Research Journal of Engineering and Environmental Sciences
Journal homepage: www.rjees.com

Original Research Article

Natural Variable Modelling and Analysis of Concentrated Non-Overlapping Winding Synchronous Reluctance Motor

***Epemu, A.M. and Nyong-Bassey, B.E.**

Department of Electrical/Electronic Engineering, College of Engineering and Technology, Federal University of Petroleum Resources Effurun, PMB 1221, Effurun, Nigeria.
*epemu.ayebatonye@fupre.edu.ng

http://doi.org/10.5281/zenodo.6720928

ARTICLE INFORMATION

Article history:
Received 13 Jan, 2022
Revised 26 Mar, 2022
Accepted 31 Mar, 2022
Available online 30 Jun, 2022

Keywords:
Natural variable model
Finite element analysis
Concentrated winding
Synchronous reluctance motor
Mathematical modelling

ABSTRACT

This study involved the modelling and analysis of a proposed line-start three-phase concentrated non-overlapping winding synchronous reluctance motor (cnWSynRM). The machine was modelled and analyzed in natural phase variables, avoiding the usage of complex matrix transformations that the usual d-q model requires. Performance characteristics such as speed, torque, inductances, phase currents, and rotor currents were measured as machine performance characteristics. The torque plot generated by the simulation revealed the presence of torque pulsations caused by the magneto-motive force (MMF) of the non-overlapping concentrated winding stator. When compared to the calculated rated torque of the motor, the proposed motor demonstrated a good torque overload capability of roughly a 36.91% increase. Although the conventional distributed winding synchronous reluctance motor is quite common due to its ability to produce better sinusoidal MMF, the proposed cnWSynRM will be easier to construct due to its fewer stator slots while still having the benefits of the concentrated winding topology. The natural variable model of the proposed machine was validated using finite element analysis (FEA), and the results were in good agreement.

1. INTRODUCTION

Synchronous reluctance machines (SynRM) are gaining popularity recently and will continue to do so because the cost of materials is much lower than that of permanent magnet machines. The SynRM is a singly-salient alternating current (AC) machine with a rotor that produces electromechanical energy using the

principle of reluctance. The hypothetical and technical description of this machine with an induction motor stator and salient-pole rotor without field-windings was first presented in Kostko, (1923). Researchers see it as a viable alternative to other AC machines due to its low manufacturing cost, simple rugged structure, high-speed capability, lack of excitation losses, short-time overload capability, and so on (Lipo 1991; Xu *et al.*, 1991; Betz *et al.*, 1993; Vagati, 1994). The SynRM's main drawbacks are its low output power, poor power factor, and poor torque (Vagati, 1994; Boglietti *et al.*, 2005).

The stator windings of electrical machines play a significant role in the production of electromagnetic torque; hence the winding configuration of an electrical machine is important. Electrical machine stator windings can be grouped as concentrated or distributed. Concentrated windings are made up of coils with non-overlapping end windings, whereas distributed windings are made up of coils with overlapping end windings. Concentrated windings can also be classified as overlapping or non-overlapping.

The concentrated non-overlapping winding topology is of interest in this study. The reason for selecting this winding type is because of its several advantages when compared to the distributed winding (Chong *et al.*, 2011; Zhao *et al.*, 2018). The primary benefits of using the concentrated non-overlapping winding topology are its compact design and non-overlapping coil ends, which result in lower copper loss, shorter axial length, and higher efficiency (Chong *et al.*, 2011; Kim *et al.,* 2014; Barre and Napame, 2015; Pop *et al.,* 2016; Dajaku *et al.*, 2017; Zhao *et al.*, 2018). Another advantage is that it has a higher fill factor, which results in a higher torque density/power density. When compared to distributed windings, this winding topology has a lower operating temperature and is less expensive, has better tolerance concerning phase faults and is easier to manufacture (Kwon *et al.*, 2006; Zhu *et al.*, 2008; Inoue *et al.*, 2011; Gundogdu *et al.*, 2014; Epemu and Obe, 2021).

A review of the underlying challenges and opportunities in the use of concentrated windings in permanent magnet machines was carried out in El-Refaie, (2009), where the author explored the vast advantages the fractional slot concentrated windings will have when used in permanent magnet motors and some challenges such as high winding harmonics. Concentrated windings have been overlooked because they produce a substantial amount of magneto-motive force (MMF) harmonics, which can cause excessive iron loss. Concentrated windings, on the other hand, are capable of producing sinusoidal MMF and EMF waveforms with the right slot and pole combinations similar to that of distributed windings (Cros and Viarouge, 2002).

Several studies have been carried out on the use of concentrated non-overlapping windings in the interior permanent magnet machine (IPM), (Libert and Soulard, 2004; Munoz and Degner, 2008; Chong *et al.*, 2008; Lee *et al.*, 2010; Vu Xuan, 2012; Yue *et al.*, 2015; Pouramin *et al.*, 2015). To the best of the knowledge of the authors no work have been carried out on the synchronous reluctance machine (SynRM) in the natural phase variables. Although in Aliyu, (2014), natural phase variable modelling of an interior permanent magnet machine having different stator topologies was done, the concentrated winding type considered in the study was the overlapping type, and the results from the study were not validated. The evidence of MMF harmonics produced by the concentrated overlapping winding topology was also not presented.

The advantages of concentrated non-overlapping windings have not been exploited in the SynRM. Most of the work on SynRM carried out have the distributed winding stator. The purpose of this paper is to model the cnWSynRM in natural phase variables and to show the feasibility of the model using FEA. It should be noted that the natural phase variable model is the modelling of the motor using the machine variables directly. The method considers only the fundamental MMF and produces the same result as the d-q model that involves complex transformations (Abdel-Halim and Manning, 1990). A similar natural phase variable method used previously was used in this study (Obe and Binder, 2011; Umoh *et al.*, 2021).

2. METHODOLOGY

2.1. Description of Motor

The concentrated stator winding reluctance motor has a dumb-bell rotor with damper windings to dampen low-frequency oscillations, presented in Figure 1(a) and a 12-slot full-pitch double-layer concentrated non-overlapping stator as seen in the winding clock diagram in Figure 1(b) was used in this study. The parameters and dimensions of the proposed machine, derived from the conventional distributed SynRM in (Obe, 2009) is presented in Table 1 and was also used for the study.

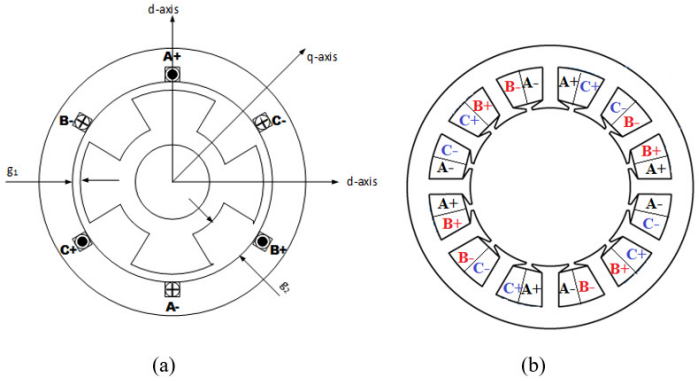

(a) (b)

Figure 1: (a) Concentrated stator winding reluctance motor (b) Winding clock diagram of the cnWSynRM

Table 1: The machine circuit parameters and dimensions

Parameter	Value	Machine dimensions	Value
Frequency (F)	50 Hz	Stator outer radius	105.2 mm
Moment of inertia (J)	0.0402 kg/m^2	Stator inner radius	67.99 mm
Winding connection	Y	Rotor radius	67.69 mm
Rated power (P_{rated})	5.5 kW	Effective stack length	160.22 mm
Rated speed	1500 rpm	Airgap length at pole face, g1	0.4 mm
Rated torque (T_{rated})	35 Nm	Airgap length between poles, g2	21.3 mm
Phase voltage (V_{ph})	370 V	Stator slot depth	18 mm
Stator resistance (R_s)	1.82 Ω	Ratio of pole arc to pole pitch	2/3
Stator leakage inductance (L_{ls})	0.256 mH	Number of Pole pairs	2
Rotor d-axis leakage inductance (L_{ldr})	2.5 mH	Number of winding layers	2
Rotor q-axis leakage inductance (L_{lqr})	3.2 mH	Number of slots	12
Rotor d-axis resistance (R_{dr})	0.12 Ω	Number of turns	96
Rotor q-axis resistance (R_{qr})	0.25 Ω	Stator slot pitch	30°

2.2. Machine Equations

The natural variable model (NVM) of the cnWSynRM is presented in this section. The mathematical model of the stator and rotor voltages of the line-start three-phase concentrated non-overlapping SynRM (cnWSynRM) are presented in their natural phases in Equations (1) and (2).

$$V_{abcs} = R_{abcs} i_{abcs} + \frac{d}{dt}\lambda_{abcs} \quad (1)$$

$$V_{qdr} = R_{qdr} i_{qdr} + \frac{d}{dt}\lambda_{qdr} \tag{2}$$

Equation (1) is the stator voltage equation, while Equation (2) is the rotor cage voltage equation. R_{abcs} represent stator resistances, i_{abcs} represent stator currents, λ_{abcs} represent stator flux linkages, R_{qdr} represent d-q rotor cage resistances, i_{qdr} represent d-q rotor currents, and λ_{qdr} represent d-q rotor flux linkages.

The parameters of Equations (1) and (2) in matrix form are:

$$V_{abcs}^{T} = [V_{as} \quad V_{bs} \quad V_{cs}] \tag{3}$$

$$V_{qdr}^{T} = [V_{qr} \quad V_{dr}] \tag{4}$$

$$R_{abcs} = diag[R_{as} \quad R_{bs} \quad R_{cs}] \tag{5}$$

$$R_{qdr} = diag[R_{qr} \quad R_{dr}] \tag{6}$$

$$i_{abcs}^{T} = [i_{as} \quad i_{bs} \quad i_{cs}] \tag{7}$$

$$i_{qdr}^{T} = [i_{qr} \quad i_{dr}] \tag{8}$$

$$\lambda_{abcs}^{T} = [\lambda_{as} \quad \lambda_{bs} \quad \lambda_{cs}] \tag{9}$$

$$\lambda_{qdr}^{T} = [\lambda_{qr} \quad \lambda_{dr}] \tag{10}$$

The flux linkage equations of the cnWSynRM stator and rotor windings are expressed in Equations (11) – (12):

$$\lambda_{abcs} = L_{abcs} i_{abcs} + L_{abcsqdr} i_{qdr} \tag{11}$$

$$\lambda_{qdr} = L_{qdr} i_{qdr} + L_{qdrabcs} i_{abcs} \tag{12}$$

The inductance matrix (L_{abcs}) comprises of the self and mutual inductances of the stator winding. L_{qdr} is the matrix having the self and mutual inductances of the rotor cage windings and $L_{abcsqdr}$ is the matrix comprising of the mutual inductances of the stator and the rotor cage windings. The variables relating to the stator and rotor windings are denoted by the subscripts *s* and *r*.

The inductances are represented in matrix form as follows:

$$L_{abcs} = \begin{bmatrix} L_{asas} & L_{asbs} & L_{ascs} \\ L_{bsas} & L_{bsbs} & L_{bscs} \\ L_{csas} & L_{csbs} & L_{csc\,s} \end{bmatrix} \tag{13}$$

$$L_{abcsqdr} = \begin{bmatrix} L_{asqr} & L_{asdr} \\ L_{bsqr} & L_{bsdr} \\ L_{csqr} & L_{csdr} \end{bmatrix} \tag{14}$$

$$L_{qdr} = \begin{bmatrix} L_{qr} & L_{qdr} \\ L_{dqr} & L_{dr} \end{bmatrix} \tag{15}$$

The diagonal components in Equation (13) contains the magnetizing and the leakage components. The main stator winding self and mutual inductances are presented in Equations (16) and (17).

$$L_{asas} = L_{la} + L_{aa0} - \sum_{k=2,4,6,\ldots}^{\infty} L_{aa1}\, cos(\, 2p_r k\theta_r - \alpha_{sk}) \tag{16}$$

$$L_{asbs} = -\frac{1}{2} L_{aao} - \sum_{k=2,4,6,\ldots}^{\infty} L_{aa1}\, cos(\, 2p_r k\theta_r - \alpha_{mk}) \tag{17}$$

The stator winding self and mutual inductances are L_{asas}, and L_{asbs}. The self-inductance also comprises of the stator leakage inductance denoted as L_{la}, k is the harmonic number, p_r is the number of pole pairs, α_{sk} and α_{mk} are the four-quadrant arctangent representing the angular displacement of each harmonic from the reference. Note L_{aa0}, and L_{aa1} are inductance constants derived from inductance plots and θ_r is the rotor angle.

The mutual inductances between the stator windings and the rotor cage winding in the q-axis and d-axis are stated as

$$L_{asqr} = \sum_{k=1,3,5,\ldots}^{\infty} L_{mq}\, cos(\, p_r k\theta_r - \alpha_{qk}) \tag{18}$$

$$L_{asdr} = \sum_{k=1,3,5,\ldots}^{\infty} L_{md}\, sin(\, p_r k\theta_r - \alpha_{dk}) \tag{19}$$

where:

$$L_{mq} = \frac{3}{2}(L_{aa0} - L_{aa1}) \tag{20}$$

$$L_{md} = \frac{3}{2}(L_{aa0} + L_{aa1}) \tag{21}$$

L_{mq} and L_{md} are the fictitious d-q axis magnetizing inductances.

Flux linkage can be stated in terms of rotor variables to stator windings (Equation 22).

$$\begin{bmatrix} \lambda_{abcs} \\ \lambda'_{qdr} \end{bmatrix} = \begin{bmatrix} L_{abcs} & L'_{abcsqdr} \\ \left(L'_{abcsqdr}\right)^T & L'_{qdr} \end{bmatrix} \begin{bmatrix} i_{abcs} \\ i'_{qdr} \end{bmatrix} \tag{22}$$

Therefore, inductance referred to the rotor parameter is given as:

$$L(\theta_r) = \begin{bmatrix} L_{abcs} & L'_{abcsqdr} \\ \frac{2}{3}\left(L'_{abcsqdr}\right)^T & L'_{qdr} \end{bmatrix} \tag{23}$$

Referring the self-inductances of the rotor cage windings to the stator will give Equation (24).

$$L'_{qdr} = \begin{bmatrix} L'_{lqr} + L_{mq} & 0 \\ 0 & L'_{ldr} + L_{md} \end{bmatrix} \tag{24}$$

The cnWSynRM electromagnetic torque equation derived from co-energy is shown in Equation (25).

$$T_{em} = \frac{p}{2} I_S^T \frac{\partial [L_s]}{\partial \theta_r} I_S \tag{25}$$

where, I_s is the stator current, p is the number of poles and L_s is the stator inductance presented in Equation (26) and (27)

$$L_s = \begin{bmatrix} L_{abcs} & L_{abcsqdr} \\ L_{abcsqdr}^T & L_{qdr} \end{bmatrix} \tag{26}$$

$$I_s = [i_{abcs} \quad i_{qdr}]^T \tag{27}$$

By substituting Equation (26) and (27) into (25), the electromagnetic torque equation (Equation 28) is obtained as the independent sum of torque produced by each stator current, showing the contribution of each winding.

$$T_{em} = \frac{p}{2} \begin{Bmatrix} i_{abcs}^T \frac{\partial L_{abcs}}{\partial \theta_r} i_{abcs} + i_{abcs}^T \frac{\partial L_{abcsqdr}}{\partial \theta_r} i_{qdr} \\ + \frac{\partial L_{abcsqdr}^T}{\partial \theta_r} i_{abcs} + i_{qdr}^T \frac{\partial L_{qdr}}{\partial \theta_r} i_{qdr} \end{Bmatrix} \tag{28}$$

The relationship between the electromagnetic torque of the machine (T_{em}) and rotor speed (ω_r) is given in the mechanical dynamic equation while ignoring the effect of friction:

$$T_{em} = J \left(\frac{2}{P}\right) p_r \omega_r + T_L \tag{29}$$

where J is the total inertia of the rotating mass, T_L is the load torque, and p_r is the number of rotor pole pairs.

2.3. Transient and Dynamic Simulation in MATLAB/Simulink

In MATLAB/Simulink, the dynamic simulation of the three-phase line-start cnWSynRM was implemented in natural phase variables using only the fundamental harmonic. The motor's circuit specifications and machine dimensions were extrapolated from a similar conventional distributed winding synchronous reluctance machine (Obe and Binder, 2011). The simulations were run at a frequency of 50 Hz and a constant supply voltage of 370 V. The magnetizing d-q inductances of the motor windings calculated from Equations (20) and (21) are L_{mq}= 9.61 mH and L_{md}=9.71 mH. The line-start cnWSynRM's initial transients and dynamic behaviour were observed. At 1 second, a load torque of 25 Nm, about (70% of rated torque) was applied to evaluate the dynamic behaviour of the model.

2.4. Finite Element Analysis in ANSYS

The transient and dynamic simulation of the proposed cnWSynRM was also done in Ansys Maxwell Electronics Desktop FEA software using the design parameters given in Table 1 for validation of the motor model. The cnWSynRM was also simulated as Line-start with a supply voltage of 370 V at a frequency of 50 Hz. The simulation time of 2 seconds was used and a 25 Nm load torque was introduced after 1 second. The speed, torque, phase currents, self and inductances, torque-speed performance characteristics of the machine were then observed and presented alongside the results gotten from the natural variable model (NVM).

3. RESULTS AND DISCUSSION

The performance characteristics of the cnWSynRM in natural phase variables and FEA are presented in this section. In Figure 2 and Figure 3, the speed characteristics of the machine model simulated in natural phase variables and FEA were presented. According to the speed plot in Figure 2, the cnWSynRM took roughly 0.28 seconds to reach a synchronous speed of 157.1 rad/s following an initial speed transient surge of 185.5 rad/s at start-up. A transient speed rise of 158.7 rad/s was recorded for the cnWSynRM after the introduction of 25 Nm load torque after 1 second which later settled at a synchronous speed of 156.8 rad/s at 1.18 seconds. The FEA speed plot of 1633 rpm showed an initial rise in speed and later settling at 1500 rpm. After 1 s of simulation, and a 25 Nm step load was introduced, the motor experienced transient disturbance before reaching steady-state at about 1500 rpm. The results demonstrate minor deviations from synchronism that is dampened after a short amount of time due to the damper windings on the rotor as seen in Figures 2 and 3.

The torque characteristic of the NVM model shown in Figure 4 did exhibit slight evidence of torque pulsations induced by MMF of the concentrated non-overlapping winding stator. At start-up, there was an initial torque rise of 179.5 Nm which settled with ripples at about 0.3 seconds. The torque ripple plot in Figure 5 was extrapolated from the torque performance plots of Figure 4. The extrapolation was done before the introduction of load torque. From the torque ripple plot of the cnWSynRM, a maximum ripple value of 5.28 Nm and a minimum ripple value of -10.46 Nm was observed.

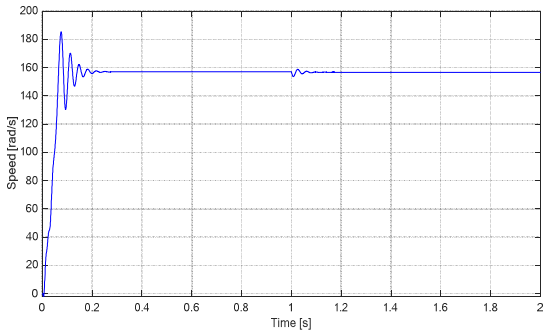

Figure 2: NVM speed against time

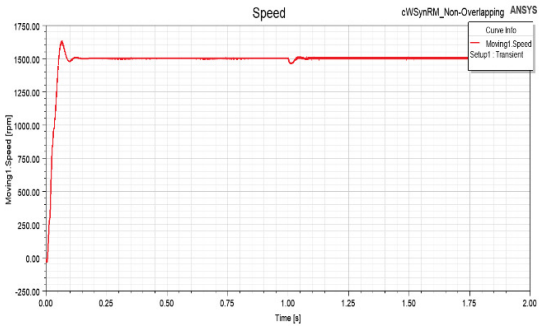

Figure 3: FEA speed against time

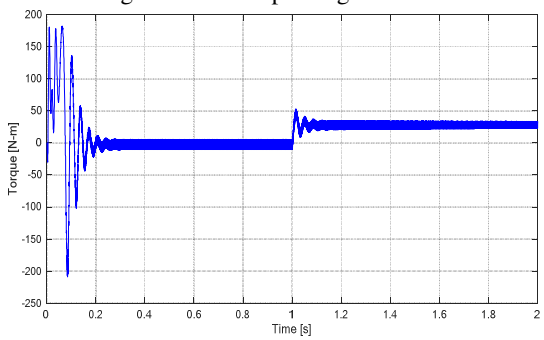

Figure 4: NVM torque against time

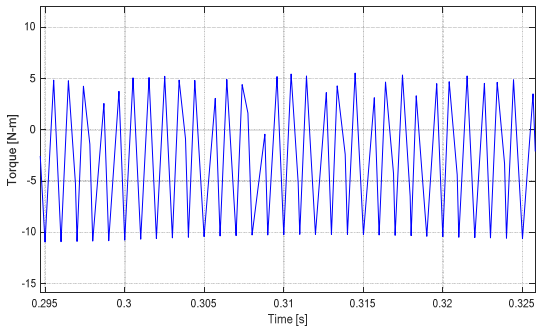

Figure 5: NVM torque against time showing ripples

The cnWSynRM FEA plot in Figure 6 had more torque pulsations or ripples in comparison to the NVM model, after a starting transient rise of about 343 Nm was observed. The cnWSynRM settled after 0.2 s with a ripple amplitude of 75 Nm. After 1s, the torque ripple increased to an amplitude of 121 Nm resulting from the application of a 25 Nm step load. The FEA torque ripple plot presented in Figure 7 was extrapolated from the torque plot of Figure 6. The extrapolation was done before the load torque was introduced. The FEA torque ripple plot of the cnWSynRM had a maximum ripple value of about 80 Nm and a minimum

ripple value of about -70 Nm was observed. The phase A self-inductances of both the NVM and the FEA models of the cnWSynRM were presented in Figures 8 and 9. The mutual inductances were shown in Figures 10 and 11. The inductance plots of the machine are essential since they define the behaviour of the cnWSynRM because it influences the SynRM's reluctance torque. The Stator phase A currents of both NVM and FEA models are shown in Figure 12 and Figure 13. The NVM current plot shows the stator winding phase A current, which is similar to the currents obtained in phases B and C, with starting transient current of 250 A and later settling at 150 A. The stator phase current of the cnWSynRM FEA plot (Figure 13) was observed as 123 A (RMS). Both plots are quite similar and in good agreement.

The torque-speed characteristics depict the relationship between the machine model's speed and torque throughout the operation phases, from start to full load speed. The torque-speed plots of Figures 14 and 15 revealed that at synchronous speed, an initial settling torque value of 0 Nm was obtained. When a load is applied, the torque value rises from 0 Nm to a settling value of 25 Nm, indicating that a full load torque is occurring at full load speed. From the FEA torque speed plot, the effects of MMF harmonics are very obvious, which is not seen in the NVM plot.

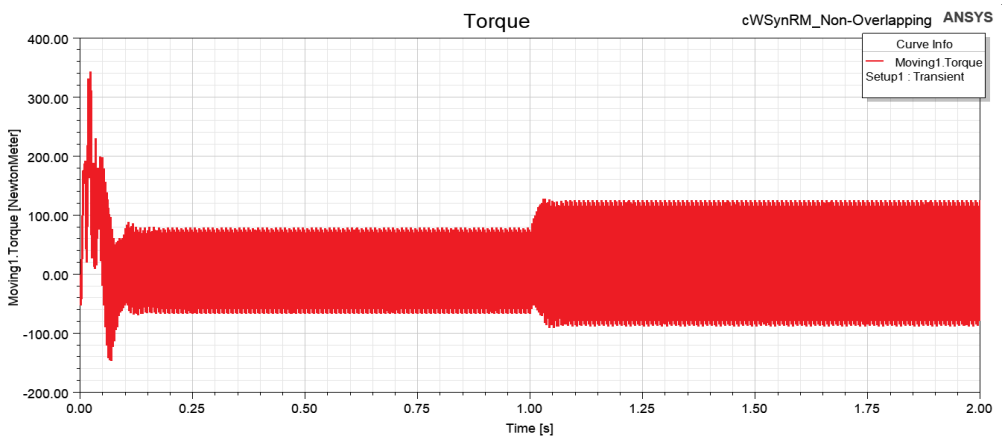

Figure 6: FEA torque against time

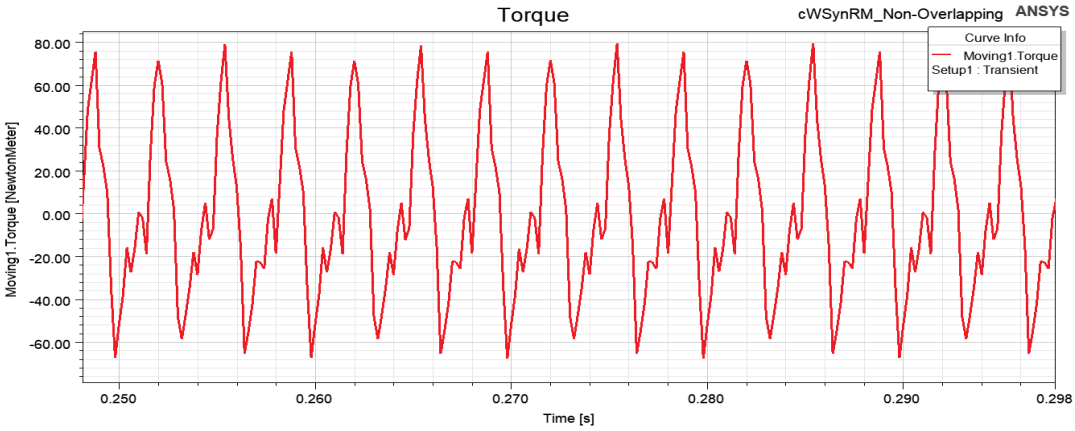

Figure 7: FEA torque against time showing ripples

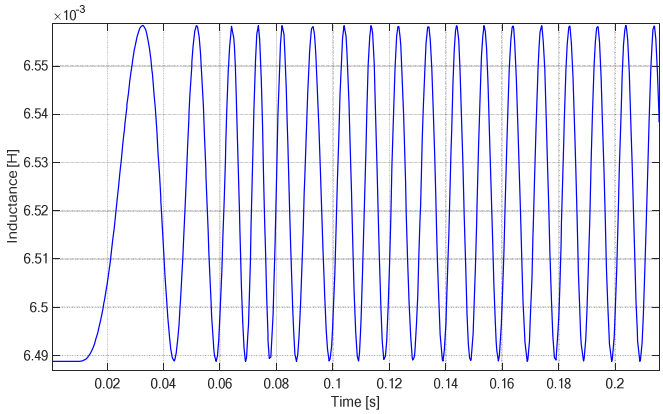

Figure 8: NVM stator self-inductance of phase A

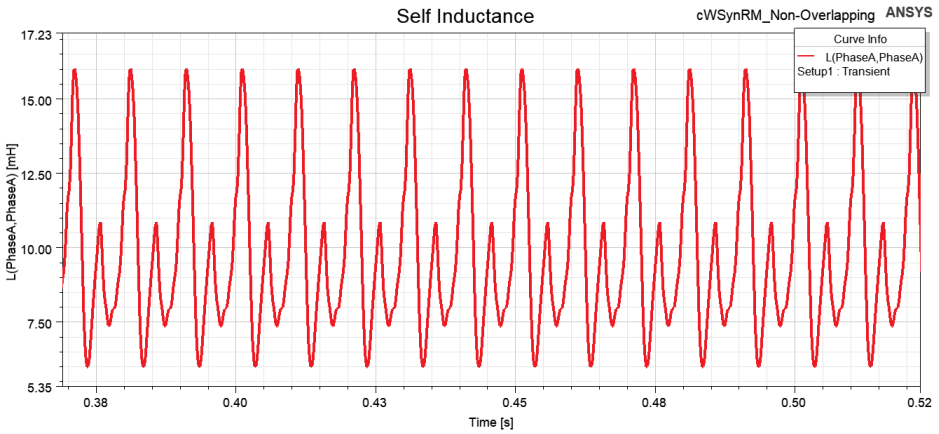

Figure 9: FEA stator self-inductance of phase A

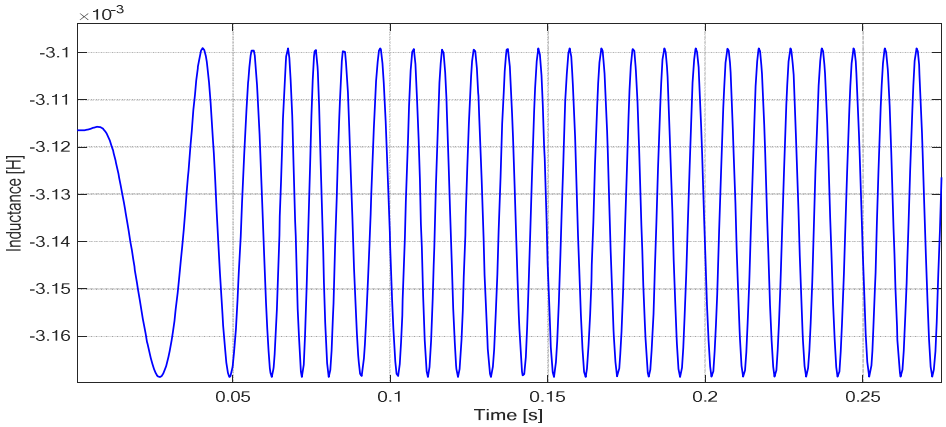

Figure 10: NVM stator mutual-inductance of phase A and phase B

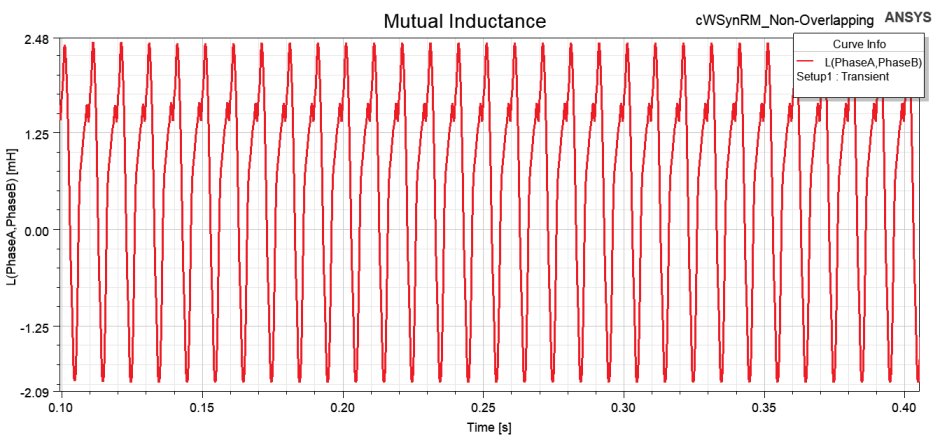

Figure 11: FEA stator mutual-inductance of phase A and B

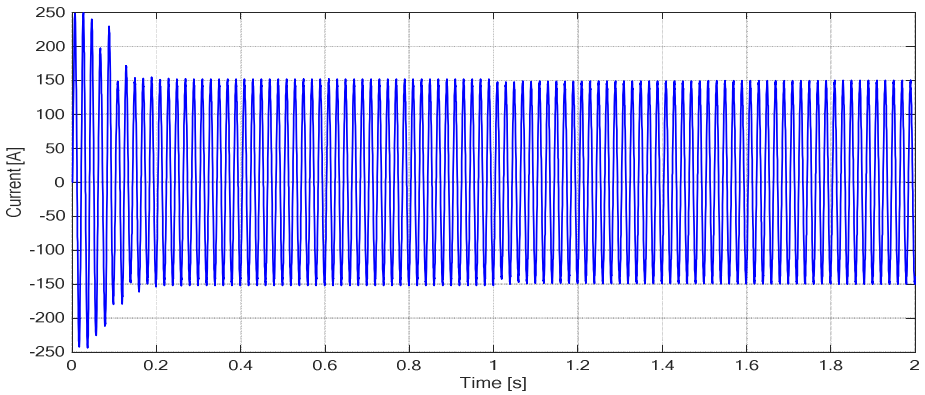

Figure 12: NVM stator winding phase A current

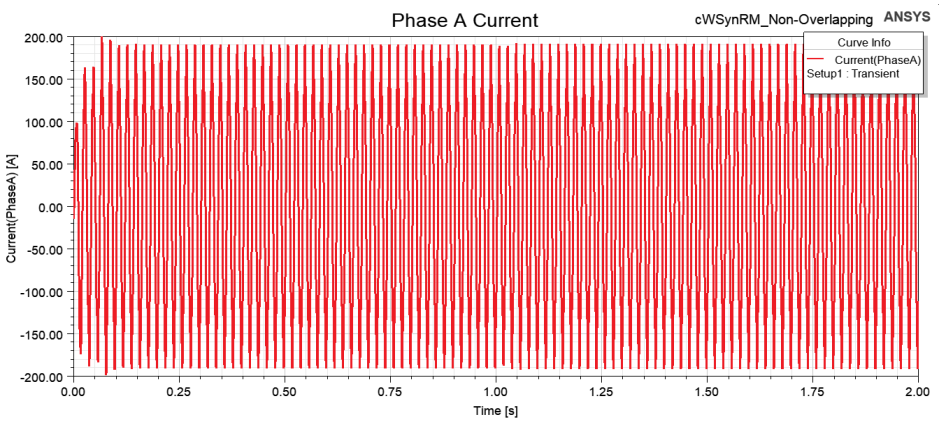

Figure 13: FEA stator winding phase A current

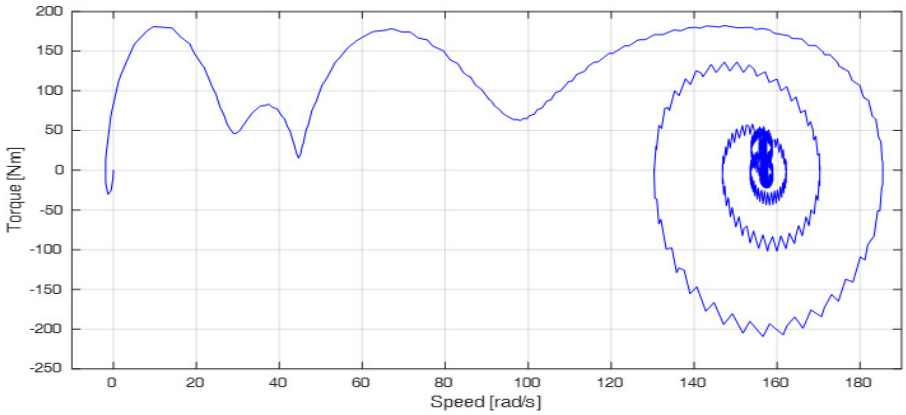

Figure 14: NVM torque-speed characteristics

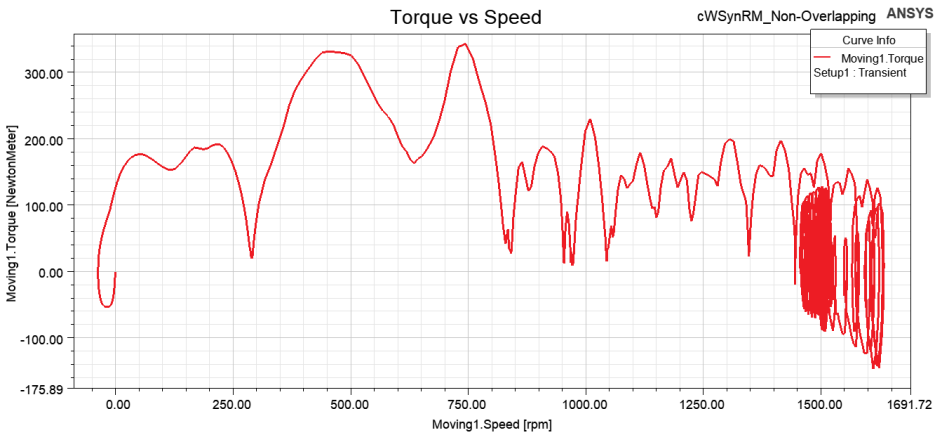

Figure 15: FEA torque-speed characteristics

The monitoring of the speed characteristic determined the loading capability of the cnWSynRM. In MATLAB/Simulink, the motor was set to Ramp load, and a load torque of 5 Nm was introduced starting at 2 seconds, as shown in Figure 16. According to Figure 17, the cnWSynRM started losing synchronism at 10.58 seconds. As a result, the cnWSynRM's maximum load torque was 47.92 Nm at 10.58 seconds. The maximum load torque was derived from the Ramp load plot (Figure 16) and the speed plot under Ramp load (Figure 17), by observing the values at 10.58 seconds when the motor lost synchronism. Synchronous reluctance motors are known to have good torque overload capability, which means the motor can keep running at load greater than the rated load. Several literatures have shown this fact (Štumberger *et al.,* 2006; Pop *et al.,* 2016; Dajaku *et al.*, 2017; Epemu and Obe, 2021).

The field plots of the cnWSynRM are presented in Figures 18 and 19. The magnetic flux density of the model presented in Figure 18 had a maximum magnetic flux density of 2.7165 T and a minimum magnetic flux density value of 0.1811 T. The magnetic vector potential of the cnWSynRM model in Figure 19 was 0.0342 Wb/m at its maximum and -0.0342 Wb/m at its minimum. These plots were derived in ANSYS using the earlier presented Maxwell's equations. The plot is not possible in MATLAB/Simulink using the NVM method. The magnetic flux densities and magnetic flux lines distributions of the cnWSynRM are visible in the plots. The field plot showed higher magnetic flux density and flux distribution on the stator laminations of the motor and also on the rotor pole face in between the damper windings.

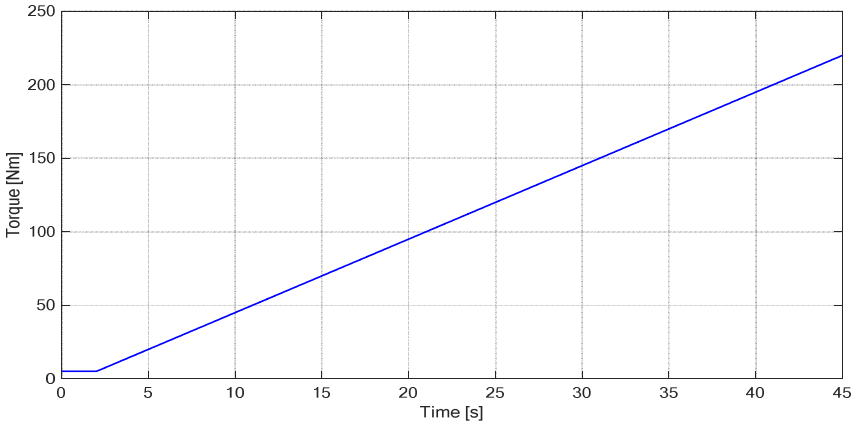

Figure 16: Ramp loading for cnWSynRM

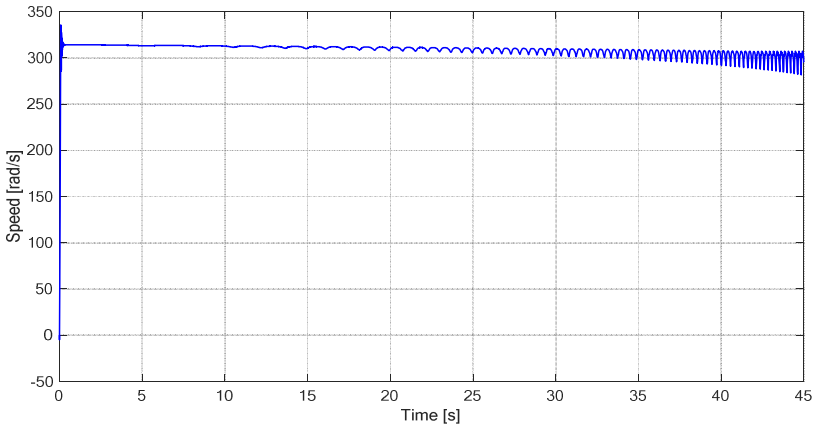

Figure 17: cnWSynRM rotor speed against time under ramp loading

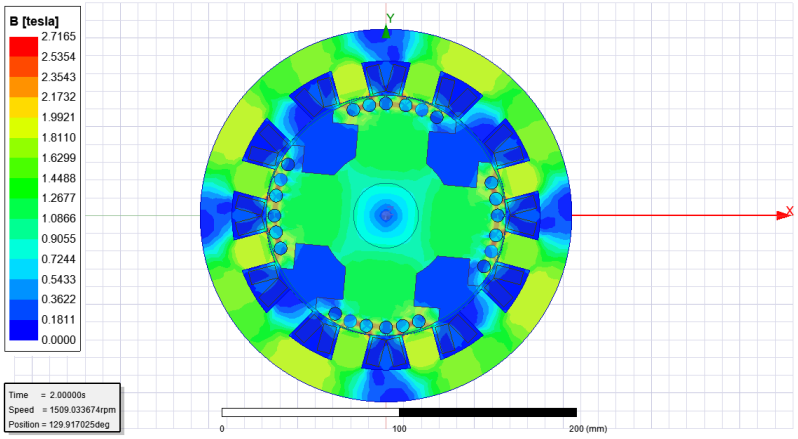

Figure 18: cnWSynRM FEA magnetic flux density magnitude

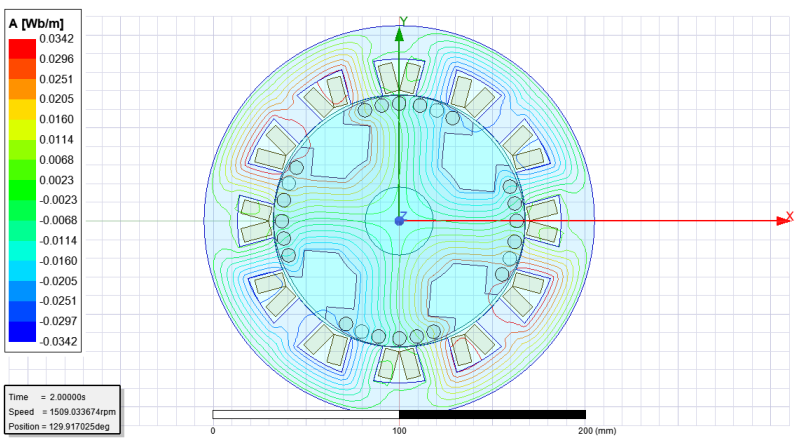

Figure 19: cnWSynRM FEA magnetic flux lines showing the magnetic vector potential

4. CONCLUSION

The natural variable model (NVM) was used to simulate the proposed concentrated non-overlapping winding synchronous reluctance motor and was validated using finite element analysis (FEA). In the NVM and FEA models, the proposed cnWSynRM was simulated as a line-start with a voltage supply of 370 V. The FEA torque plots revealed more torque pulsations caused by the concentrated stator winding, which would not be visible in the NVM. Although the FEA model validated that the cnWSynRM is viable and also presented the evidence of MMF harmonics in its results, meaning its more accurate, it does not invalidate the results from the NVM as both results are in good agreement. When compared to the rated torque, the simulation showed that cnWSynRM could tolerate a 36.91% increase in torque overload. The concentrated winding SynRM will be easier to construct because it has fewer slots than the traditional distributed winding SynRM. The key rewards of using the concentrated winding topology, such as reduced axial length, compact design, and shorter coil-ends, which result in lower copper losses and higher efficiency, was taken advantage of. Hence the proposed machine is viable and can be used in constant-speed applications and also as pumps in the oil and gas industry. The study also implies that the natural phase model can be used in other AC machines analysis because it provides some form and accuracy without requiring complex transformations as seen in the popular conventional d-q model. The FEA results obviously validated the NVM model when the performance characteristics of the cnWSynRM were compared. This proves that the cnWSynRM is feasible.

5. ACKNOWLEDGMENT

The authors acknowledged the financial support received from the Petroleum Technology Development Fund (PTDF) under scholar no. PTDF/ED/LSS/PHD/AME/142/17.

6. CONFLICT OF INTEREST

There is no conflict of interest associated with this work.

REFERENCES

Abdel-Halim, M. A. and Manning, C. D. (1990). Direct phase modelling of synchronous generators. *IEEE Proceedings B (Electric Power Applications)*, 137(4), pp. 239–247.

Aliyu, N. (2014). Natural Variable Modeling and Performance of Interior Permanent Magnet Motor with Concentrated and Distributed Windings. MSc. Thesis Dept. of Electrical Engineering, University of Nigeria.

Barre, O. and Napame, B. (2015). Fractional slot concentrated windings: a new method to manage the mutual inductance between phases in three-phase electrical machines and multi-star electrical machines. *Machines*, *3*(2), pp. 123-137.

Betz, R. E., Lagerquist, R., Jovanovic, M., Miller, T. J. and Middleton, R. H. (1993). Control of synchronous reluctance machines. *IEEE Transactions on Industry Applications*, *29*(6), pp. 1110-1122.

Boglietti, A., Cavagnino, A., Pastorelli, M. and Vagati, A. (2005). Experimental Comparison of Induction and Synchronous Reluctance Motors Performance. *Proceedings of IEEE Industry Applications Conference, October 2 – 6, 2005, Hong Kong, China.* pp. 474–479.

Chong, L., Dutta, R. and Rahman, M. F. (2008). Application of concentrated windings in interior permanent magnet machine. *Australian Journal of Electrical and Electronics Engineering*, 5(3), pp. 229–236.

Chong, L., Dutta, R. and Rahman, M.F. (2011). Performance Comparison between Concentrated and Distributed Wound IPM Machines used for Field Weakening Applications. *Proceedings of International Aegean Conference on Electrical Machines and Power Electronics and Electromotion, Joint Conference, September 8 – 10, 2011, Istanbul, Turkey*. pp. 8–10.

Cros, J. and Viarouge, P. (2002). Synthesis of High-Performance PM Motors With Concentrated Windings. *IEEE transactions on energy conversion*, 17(2), pp. 248–253.

Dajaku, G., Bilyi, V. and Gerling, D. (2017). Feasibility analysis of an improved FSCW for synchronous reluctance traction machines. In: *IEEE International Electric Machines and Drives Conference (IEMDC)*, *May 21 – 24, 2017, Florida, USA*. pp. 1-7.

El-Refaie, A.M. (2009). Fractional-slot concentrated-windings synchronous permanent magnet machines: Opportunities and challenges. *IEEE Transactions on Industrial Electronics*, 57(1), pp. 107–121.

Epemu, A. M. and Obe, E.S. (2021). Performance Evaluation of Synchronous Reluctance Motors with different Concentrated Stator Winding Topologies. *Proceedings of the 2nd International Conference on Electrical Power Engineering (ICEPENG 2021), May 18 – 22, 2021, Nsukka, Nigeria*, pp. 5–10.

Gundogdu, T., Komurgoz, G. and Mantar, B. (2014). Implementation of fractional slot concentrated windings to Induction Machines. *Proceedings of 7th IET International Conference on Power Electronics, Machines and Drives (PEMD 2014), April 8 – 10, 2014, Manchester, UK.* pp. 1–6.

Inoue, M., Kuroda, Y., Nishimura, S. and Akita, H. (2011). An evaluation of concentrated and distributed windings in interior PM and claw pole motors. *Proceedings of IEEE 8th International Conference on Power Electronics-ECCE Asia, May 30 – June 3, 2011, Jeju, South Korea.* pp. 176–183.

Kim, H. J., Kim, D. J. and Hong, J. P. (2014). Characteristic analysis for concentrated multiple-layer winding machine with optimum turn ratio. *IEEE transactions on magnetics*, *50*(2), pp. 789-792.

Kostko, J.K. (1923). Polyphase reaction synchronous motors. *Journal of the American Institute of Electrical Engineers*, 42(11), pp. 1162–1168.

Kwon, S., Kim, S., Zhang, P. and Hong, J. (2006). Performance comparison of IPMSM with distributed and concentrated. *Proceedings of IEEE Conference on Industrial Electronics, October 8 – 12, 2006, Florida, USA*. pp. 1984–1988.

Lee, J.J., W. Kim, W. H., Yu, J. S., Yun, S. Y. and Kim, S.M. (2010). Comparison between concentrated and distributed winding in IPMSM for traction application. *Proceedings of International Conference on Electrical Machines and Systems, October 10 – 13, 2010, Incheon, South Korea.* pp. 1171–1174.

Libert, F. and Soulard, J. (2004). Investigation on pole-slot combinations for permanent-magnet machines with concentrated windings. *Proceedings of International Conference of Electrical Machines (ICEM), September 5 – 8, 2004, Cracow, Poland*, (4), pp. 5-8.

Lipo, T. A. (1991). Synchronous reluctance machines-a viable alternative for ac drives. *Electric Machines and Power Systems*, *19*(6), pp. 659-671.

Muñoz, A.R. and Degner, M.W. (2008). Evaluation of Interior PM and Surface PM Synchronous Machines with Distributed and Concentrated Windings. *Proceedings of IEEE International Conference on Industrial Electronics*, pp. 1189–1193.

Obe, E.S. (2009). Direct computation of ac machine inductances based on winding function theory. *Energy Conversion and Management*, 50(3), pp. 539–542.

Obe, E. S. and Binder, A. (2011). Direct-phase-variable model of a synchronous reluctance motor including all slot and winding harmonics. *Energy Conversion and Management*, 52, pp. 284–291.

Pop, F. P., Marțiș, R., Dărămus, A., Marțiș, C., Pop, A. C. and Vintiloiu, I. (2016, October). Design and analysis of slot-pole combination for synchronous reluctance machine with concentrated windings for automotive applications. *International Conference and Exposition on Electrical and Power Engineering (EPE), October 20 – 22, 2016, Iasi, Romania.* pp. 229-234.

Pouramin, A., Dutta, R., Rahman, M. F. and Xiao, D. (2015). Inductances of a Fractional-Slot Concentrated- Winding Interior PM Synchronous Machine Considering Effects of Saturation and Cross Magnetization. *Proceedings of IEEE Energy Conversion Congress and Exposition (ECCE), September 20 – 24, 2015, Montreal, Canada.* pp. 6075–6081.

Štumberger, G., Hadžiselimović, M., Štumberger, B., Miljavec, D., Dolinar, D. and Zagradišnik, I. (2006). Comparison of capabilities of reluctance synchronous motor and induction motor. *Journal of Magnetism and Magnetic Materials*, *304*(2), pp. 835-837.

Umoh, G., Obe, C., Ogbuka, C., Ekpo, G. and Obe, E. S., (2021). Direct-phase variable modelling and analysis of five-phase synchronous reluctance motor for direct-on-line starting. *Przegląd Elektrotechniczny*, 97(1), pp. 24–29.

Vagati, A. (1994). The synchronous reluctance solution: A new alternative in AC drives. *Proceedings of IECON'94-20th Annual Conference of IEEE Industrial Electronics*, 1*, September 5 – 9, 1994, Bologna, Italy*. pp. 1–13.

Vu Xuan, H. (2012). Modelling of exterior rotor permanent magnet machines with concentrated windings" PhD. Dissertation, Sch. of Eng., Delft University of Technology, The Netherlands.

Xu, L., Xu, X., Lipo, T. A. and Novotny, D. W. (1991). Vector control of a synchronous reluctance motor including saturation and iron loss. *IEEE transactions on industry applications*, *27*(5), pp. 977-985.

Yue, L., Yulong, P., Yanjun, Y., Yanwen, S. and Feng, C. (2015). Increasing the saliency ratio of fractional slot concentrated winding interior permanent magnet synchronous motors. *IET Electric Power Applications*, 9(7), pp. 439–448.

Zhao, J., Liu, Y. and Xu, X. (2018). Comparisons of Concentrated and Distributed Winding PMSM in MV Power Generation. *Proceedings of 2018 XIII International Conference on Electrical Machines (ICEM)*, September 3 – 6, 2018, Alexandroupoli, Greece. pp. 2437–2443.

Zhu, D., Qiu, X., Zhou, N. and Yan, Y. (2008). A Comparative Study of Winding Factors between Distributed Windings and Non- overlapping Concentrated Windings. *Proceedings of International Conference on Electric Utility Deregulation and Restructuring and Power Technologies*, *April 6 – 9, 2008, Nanjing, China*. pp. 2725–2729.